SEBASTIAN RULIK[1], *WŁODZIMIERZ WRÓBLEWSKI*[1], *KRZYSZTOF RUSIN*[1]

A NUMERICAL STUDY OF THE RELATION BETWEEN THE ACOUSTIC GENERATOR GEOMETRY AND THE HEAT TRANSFER CONDITIONS

Modern gas turbine systems operate in temperatures ranging from 1200°C to even 1500°C, which creates bigger problems related to the blade material thermal strength. In order to ensure appropriate protection of the turbine blades, a sophisticated cooling system is used. Current emphasis is placed on the application of non-stationary flow effects to improve cooling conditions, e.g., the unsteady-jet heat transfer or the heat transfer enhancement using high-amplitude oscillatory motion. The presented research follows a similar direction.

A new concept is proposed of intensification of the heat transfer in the cooling channels with the use of an acoustic wave generator. The acoustic wave is generated by an appropriately shaped fixed cavity or group of cavities. The phenomenon is related to the coupling mechanism between the vortex shedding generated at the leading edge and the acoustic waves generated within the cavity area. Strong instabilities can be observed within a certain range of the free flow velocities.

The presented study includes determination of the relationship between the amplitude of acoustic oscillations and the cooling conditions within the cavity. Different geometries of the acoustic generator are investigated. Calculations are also performed for variable flow conditions. The research presented in this paper is based on a numerical model prepared using the Ansys CFX-17.0 commercial CFD code.

Nomenclature

f — frequency, Hz

HTC — heat transfer coefficient, W/(m^{2}K)

k — ratio between the vortex convection and the free flow velocity

[1]*Institute of Power Engineering and Turbomachinery, Silesian University of Technology, 44-100 Gliwice, Konarskiego 18 Str. Emails: sebastian.rulik@polsl.pl, wlodzimierz.wroblewski@polsl.pl, krzysztof.rusin@polsl.pl*

k_e	turbulence kinetic energy, J/kg
m	mode number
M	Mach number
n	number of time steps
u	horizontal component of velocity, m/s
L	cavity or cavity neck length, m
D	cavity depth, m
a	sound velocity, m/s
h	specific enthalpy, kJ/kg
p	pressure, Pa
r_c	recovery factor
St	Strouhal number
t	time, s
T	temperature, K

Greek symbols

λ	wave length, m
α	phase shift between vortices
μ	dynamic viscosity, Pa·s
κ	specific heat ratio
ω	turbulence frequency, 1/s
τ	shear stress, kPa
δ	unit tensor

Subscripts

w	vortex
wall	walls
ad	adiabatic
a	sound
avg	average
∞	free flow
c	convection
ins	instantaneous
tot	total
eff	effective

1. Introduction

An improvement in the heat transfer conditions is the key issue in the operation of different kinds of machinery and equipment, especially in power engineering. On the one hand, a rise in the heat transfer coefficient improves the energy conversion

efficiency. On the other – it makes it possible to achieve more compact dimensions of machines and devices. Considering the power engineering sector, two key areas can be distinguished where an improvement in the heat transfer conditions is of vital significance. One of them comprises the gas turbine cooling system. As gas turbines now operate in very high temperatures of 1200–1500°C, new more efficient cooling methods have to be found. The other area comprises the heat transfer phenomenon in membrane heat exchangers, e.g., shell-and-tube heat exchangers. The heat transfer intensification concept presented herein can be used for these particular elements, but it can also be applied in other structures subjected to thermal loads.

Generally, the main direction of the search for methods improving the heat transfer between a fluid characterized by specific parameters and flowing through a channel and the channel wall concentrates on modifying the wall shape to achieve a geometry that will involve a rise in the heat transfer coefficient value. An example of such modification is to fix a series of elements, e.g., ribs, fins, pins or any kind of projections, on the wall surface to turbulize the flow. It is also possible to increase the fluid flow velocity or alter the flow direction. The flow becomes turbulent, which involves a rise in the heat transfer coefficient values at the expense of a bigger drop in pressure. For this reason, research on other methods of intensifying the heat transfer in channels, e.g., by generating a highly non-stationary flow field, is so important.

Many publications present numerical or experimental analyses where different configurations of flow-turbulizing elements are investigated. Examples of experimental testing of flows through a straight, ribbed channel and through a ribbed channel with additional protrusions are described in [1]. The impact of protrusions and of their arrangement on the flow field structure and, consequently, on the conditions of the heat transfer in cooling channels is also presented in [2, 3]. The problem of the heat transfer intensification in U-shaped channels used in the system of convective cooling of the gas turbine blade is discussed in [4]. The works mentioned above focus exclusively on stationary effects of the impact of additional turbulizers on the flow field structure. The other group of current intense researches concentrates on methods aiming at improving the heat transfer conditions using non-stationary effects. A good example is impingement cooling using a non-stationary cooling jet [5–7]].

The research presented herein follows a similar direction. It concentrates on the application of an acoustic wave, being a source of considerable non-stationary effects, to intensify the heat transfer in channels. The relation between pressure pulsations associated with the generation of acoustic waves and intensification of heat transfer process is not currently studied by other authors. Conducted research are aimed towards experimental analysis and numerical modeling of the noise generation and propagation process [8, 9]. From this point of view, the presented paper is a new approach which associates aeroacoustic with heat transfer conditions.

The research is an extension of the works presented in [10] and [11]. The first paper presents preliminary analyses of the possibility of improving cooling

conditions in U-shaped channels, whereas the second one concerns a detailed analysis of the applied numerical model, together with the model validation and determination of the impact of the flow velocity on cooling conditions. The focus of the research presented in this paper is to define the relation between basic geometrical parameters of the acoustic generator and the parameters of the generated acoustic wave, and to determine the impact of the parameters on the heat transfer process.

In the presented studies, a properly shaped cavity is an acoustic generator. Investigation of heat transfer process in the case of flow over the cavity is also important, because similar type of flow phenomena can be found especially in the case of turbomachinery, e.g., flow through the labyrinth seals [12] or flow between the guide vane carriers and the casing of industrial steam turbines [13].

2. Heat transfer intensification using an acoustic wave generator

It is proposed herein that the heat transfer in channels should be intensified by means of an acoustic generator in the form of an appropriately shaped cavity or group of cavities. If the flow conditions are selected correctly, an acoustic wave is generated. The effect of the wave is that the flow field within the cavity or in its immediate vicinity becomes highly non-stationary. The idea of the proposed solution is illustrated in Fig. 1.
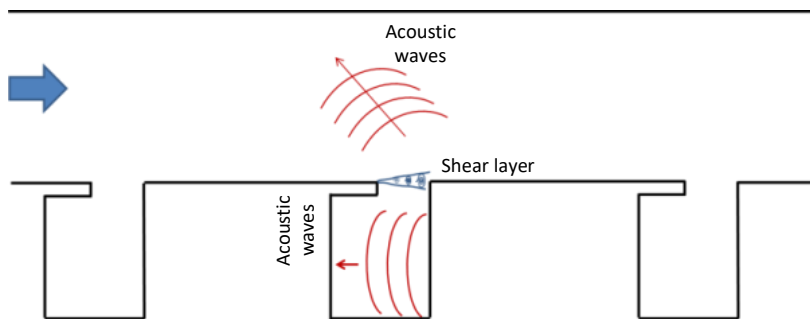

Fig. 1. Diagram illustrating the idea of the application of a group
of acoustic generators intensifying the heat transfer

In the proposed solution, the channel wall is perforated using appropriately shaped longitudinal cavities. The fluid jet gets separated on the leading edge of each cavity, and vortices are generated. The vortices reach the cavity trailing edge, hit it and flow down one by one. The flow of the vortices generates an acoustic wave which travels inside the cavity in the direction opposite to the flow direction. As a result, new vortices are formed and their flow is more intense. For this reason, the frequency at which vortices flow in the cavity open neck should correspond to that of the generated acoustic wave. This can be expressed using the following

relation [14, 15]:

$$f = \frac{ku_\infty}{\lambda_v} = \frac{a}{\lambda_a},$$ (1)

where k is the ratio between the vortex convection velocity and the free-flow velocity u_∞, and λ_v and λ_a are the wave lengths directly related to the vortices flowing in the cavity neck area and to the generated acoustic wave, respectively.

The mechanism of the feedback between the vortices and the acoustic wave was first described by Rossiter [14], who put forward a simple model that makes it possible to determine the phenomenon resonance frequencies using the following relation:

$$St = \frac{fL}{U_\infty} = \frac{m - \propto}{M + \frac{1}{k}} \qquad m = 1, 2, 3,$$ (2)

where f is the pressure fluctuation frequency and L is the cavity length. M is the Mach number, and quantity α is the phase shift between the moment of the vortex impact against the cavity rear wall and the moment of the acoustic wave generation. Quantities k and α are usually selected empirically [15].

The other mechanism of the acoustic wave generation can be the work of the presented system operating as the Helmholtz resonator [16]. The mechanism is characteristic of cavities with a lid, such as the ones presented in Fig. 1.

The presented testing concerns the phenomena occurring in a single cavity. If a group of cavities is analysed, it is essential that the interference of the generated acoustic waves is taken into consideration because the phenomenon may contribute to changes in operating parameters of individual acoustic generators.

3. Applied numerical model

The research presented herein was conducted based on a numerical model developed by means of the Ansys CFX 16 code. The software uses an implicit finite-volume formulation to solve discretized unsteady Reynolds-averaged Navier-Stokes equations (URANS) for the compressible fluid flow [10]. The governing equations are the mass, momentum and energy conservation laws:

$$\frac{\partial \rho}{\partial t} + \nabla \cdot (\rho \, \mathbf{v}) = 0,$$ (3)

$$\frac{\partial (\rho \, \mathbf{U})}{\partial t} + \nabla \cdot (\rho \, \mathbf{v} \otimes \mathbf{v}) = -\nabla p + \nabla \cdot \boldsymbol{\tau},$$ (4)

$$\frac{\partial (\rho h_{tot})}{\partial t} - \frac{\partial p}{\partial t} + \nabla \cdot (\rho \, \mathbf{v} \, h_{tot}) = \nabla \cdot (\lambda \nabla T) + \nabla \cdot (\mathbf{v} \cdot \boldsymbol{\tau}).$$ (5)

The presented equation takes no account of the impact of displacement effects. The relation between stress tensor τ and the strain rate is expressed as:

$$\tau = \mu_{eff}\left(\nabla\mathbf{v} + (\nabla\mathbf{v})^T - \frac{2}{3}\delta\nabla\cdot\mathbf{v}\right). \tag{6}$$

In equation (5), term $\nabla\cdot(\mathbf{v}\cdot\boldsymbol{\tau})$ represents the work due to viscous stresses and is referred to as the viscous work term.

Turbulence is modelled using the two-equation Shear Stress Transport (SST) turbulence model proposed by Menter [17]. It is a combination of two turbulence models, thus combining the advantages of the Wilcox $k - \omega$ model near the wall and the standard $k - \varepsilon$ model in what is referred to as the far field. A detailed description of the applied turbulence model can be found in [17] and [18].

High-resolution spatial discretization scheme was applied for solution of the presented equations. The second-order accuracy Euler scheme was used for integration with respect to time. The transient simulation was conducted using basic time step that equals 10^{-5} s. This corresponds to 85 iterations per one full period of pressure pulsation inside the cavity. According to [19], this amount is sufficient to provide correct modeling of acoustic wave propagation.

The analyzed computational area and the adopted boundary conditions are presented in Fig. 2. It is a flow channel with the height of 40 mm and length $40D_1$ ($D_1 = 50.84$ mm – for the reference cavity). A single cavity is located on the channel bottom wall in the middle of the channel length. The cavity is partly
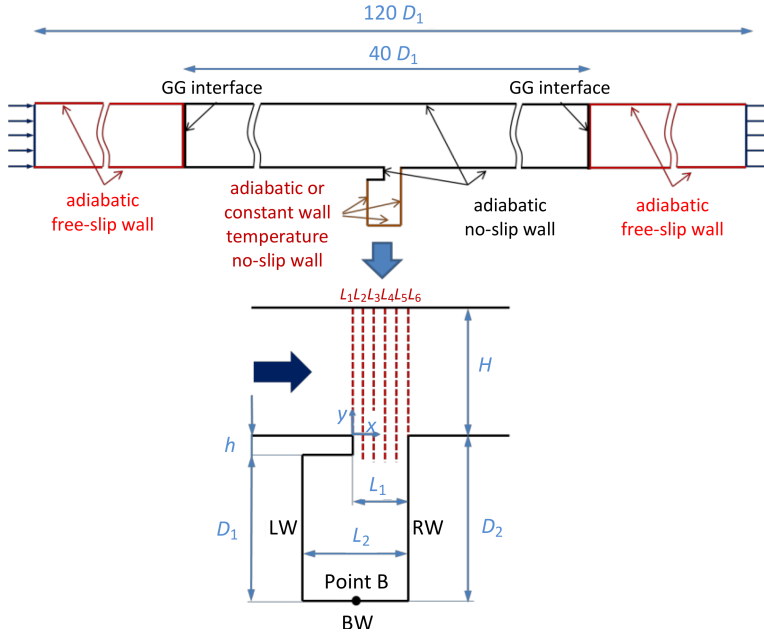

Fig. 2. Numerical model applied in the analysis

covered at the inlet and its L_1/D_2 ratio is 0.56. It is assumed that the computational area is 1 mm wide. For this reason, the conducted CFD analysis should be treated as a two-dimensional one.

In the presented model, the symmetry boundary condition is assumed for the channel lateral walls, and the no-slip wall boundary condition is adopted for the channel bottom and top surfaces.

Two additional areas are used: one at the channel inlet and the other – at the outlet. They are joined to the channel area by means of the General Grid Interface. A relatively thin numerical mesh is used. Due to that, the acoustic waves moving along channels are subject to gradual attenuation in this place. Such a solution prevents potential reflection of acoustic waves – a phenomenon that might make the computational process unstable.

In the additional areas, the free-slip wall boundary condition is assumed for the bottom and top surfaces of the channel. As a result, the area does not generate additional losses in the flow channel.

Fig. 3 presents a detail of the numerical mesh adopted for the CFD computations in the cavity inlet area. It is a structural, orthogonal mesh with 231 thousand nodes. Depending on the variants of the analysed geometry, the number is varied slightly to keep the same level of discretization in all places which are essential for the course of the phenomenon.
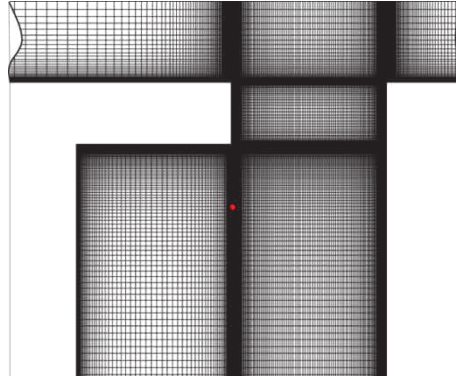

Fig. 3. Detail of the numerical mesh adopted for the CFD analysis

Due to the assumed symmetry of the flow, the computational domain width is discretized using a single element, which corresponds to a two-dimensional flow analysis. The numerical mesh is denser in the cavity neck area. For all walls of both the channel and the cavity, the non-dimensional distance takes the value of $y^+ \approx 1$. The mesh density decreases gradually towards the channel inlet and outlet. In the interface area there is a jump change in the size of the numerical mesh elements, while in the additional area the mesh density is not increased along the channel edge due to the assumed boundary condition of a free-slip wall. The basic boundary conditions and the numerical simulation parameters are listed in Table 1.

Table 1.

Boundary conditions and basic assumptions for the CFD analysis

INLET	Velocity: 50 m/s Static temperature: 288.15 K Turbulence intensity: 1%
OUTLET	Averaged static pressure: 1 bar
Channel walls	Adiabatic
Cavity walls	Adiabatic or heat transfer with constant wall temperature equal to 393.15 K
Fluid	Air ideal gas
Heat transfer	Total Energy option
Turbulence model	SST

An analysis of the solution independence of the applied numerical mesh is presented in detail in [11].

4. Numerical analysis results

The testing of the acoustic wave generation and propagation requires transient numerical simulations. The fact that the numerical model takes additional account of the heat transfer between the fluid and the cavity walls complicates the computational process significantly due to different time scales of the phenomena under analysis. On the one hand, it is necessary to ensure appropriate time discretization for the modelling of the acoustic wave behaviour; on the other – an appropriate length of time is required to achieve a steady and periodically changing heat flux transferred through the cavity walls. Considering this, the computations were divided into two phases. The first was devoted exclusively to the acoustic wave generation and propagation, taking no account of the heat transfer process. The focus here was on the analysis of the generated acoustic wave basic parameters, such as amplitude and frequency. In the second phase, the variant with the highest value of the amplitude of the acoustic wave oscillations was selected and analysed in detail, taking the heat transfer into consideration.

This paper concentrates on determination of the impact of the acoustic generator basic dimensions on the parameters of the generated acoustic wave and, subsequently, on the heat transfer intensification in the cavity area. The considered configurations of the acoustic generator are presented in Fig. 4. In total, the analysis covered ten different geometries. The initial geometry, marked as G1, was also analysed in detail in [11]. For configurations G2–G9, the cavity most essential geometrical parameters were varied: depth D1, neck height H, neck width L1 and the width of the entire cavity L2. Each modified characteristic dimension was equal to 80 or 120% of the initial dimension. Based on the obtained results, the acoustic generator modified geometry (G10) is proposed. A numerical analysis is carried
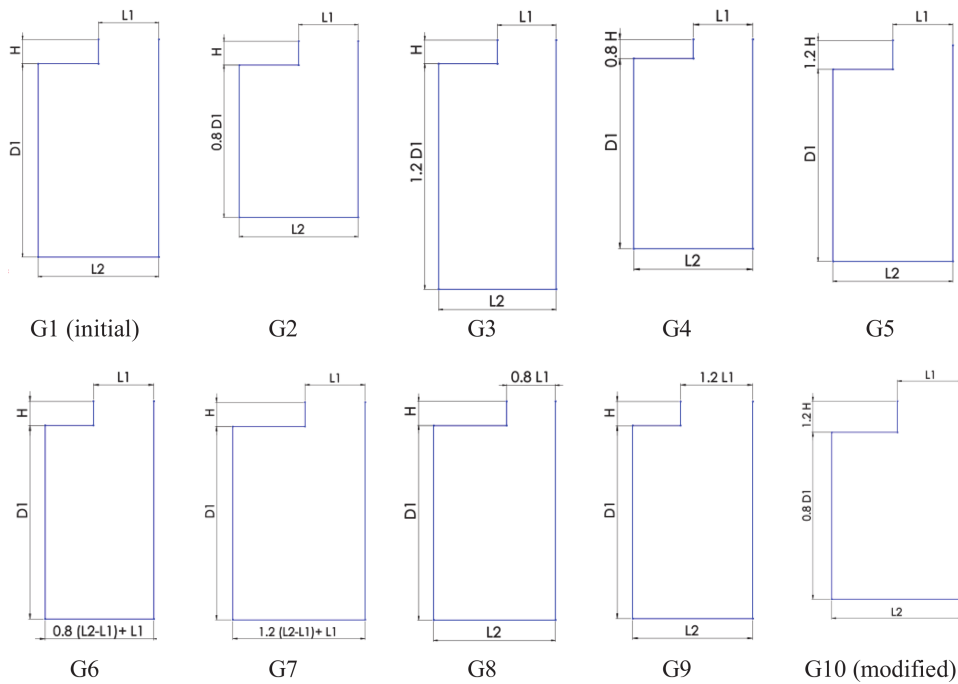
Fig. 4. Geometries of the acoustic generator considered in the analysis

out for this configuration in the further part of this paper, taking account of the heat transfer through the cavity walls.

Absolute dimensions of the cavity individual configurations are listed in Table 2. The cavity geometry is scaled with factor 2 compared to the experimental testing presented in [20]. The problem of scale in studies on this particular phenomenon is analysed in many works, both numerical and experimental [21, 22].

Table 2.
Characteristic dimensions of the acoustic generator configurations under analysis

Geometry	D_1, mm	h, mm	L_2, mm	L_1, mm
G1	50.84	6.36	31.76	15.88
G2	40.67	6.36	31.76	15.88
G3	61.01	6.36	31.76	15.88
G4	50.84	5.09	31.76	15.88
G5	50.84	7.63	31.76	15.88
G6	50.84	6.36	28.58	15.88
G7	50.84	6.36	34.94	15.88
G8	50.84	6.36	28.58	12.70
G9	50.84	6.36	34.94	19.06
G10	40.67	7.63	31.76	15.88

The increase in the cavity size was dictated by the need to adjust the dimensions so that they could be tested on the constructed laboratory stand. The use of a bigger cavity makes it easier to prepare appropriate heating elements. It also enables better metering of the testing stand and improves the accuracy of the measurements. The tested device will be gradually miniaturized in further stages of the works. It is worth noting here that, if the flow velocity is kept the same and the device is scaled gradually, the Strouhal number remains almost constant. This means that a rise in the generated acoustic wave frequency is proportional to the decrease in the size of the entire cavity provided that the ratios between the cavity characteristic dimensions are kept identical.

The first part of the testing is the non-stationary flow field analysis conducted for the presented configurations of the acoustic generator with no account taken of the heat transfer in the cavity area. The obtained results are presented in Fig. 5 and Fig. 6. Fig. 5 presents an FFT analysis of fluctuations in pressure and in the sound pressure level for point B, located close to the middle of the cavity bottom wall, as presented in Fig. 2. Fig. 6 presents the RMS value of the normalized value of fluctuations in the horizontal component of velocity. They were calculated using the following formula:

$$u'_{rms} = \sqrt{\frac{\sum\limits_{i=1}^{n}(u_{ins} - u_{\mathrm{avg}})^2}{n}}, \tag{7}$$

where: n – number of time steps, u_{ins} – instantaneous local velocity value, m/s, u_{avg} – average local velocity value calculated based on n time steps, m/s.

To determine the RMS value of velocity fluctuations, data from the last 4200 iterations were analyzed, which corresponds to 50 full periods of pressure pulsation inside the acoustic generator.

Except for configurations G3 and G8, in all the cases under analysis the obtained amplitude of acoustic oscillations was significant, with a well visible fundamental component. The obtained value of the fundamental component of the generated acoustic wave frequency spectrum is similar in each case and it is included in the range of 1074–1196 Hz, which corresponds to period of time between 0.84–0.93 ms. The highest amplitude of acoustic oscillations of 216 Pa, which corresponds to 141 dB, was obtained for configuration G2, where the cavity vertical dimension is reduced by 20%. A significant rise in the oscillation amplitude was also obtained for configuration G5, where the vertical dimension of the cavity neck is increased by 20%. The lowest value of the sound pressure level was obtained for configurations G3 and G8. In both cases it totals about 78 dB, but it is only in configuration G3 that the fundamental component is clearly visible.

Except for configuration G8, all the curves illustrating the pressure pulsations have a sinusoidal character with a well visible fundamental component and much smaller values of the amplitude of the other harmonic components. Taking account
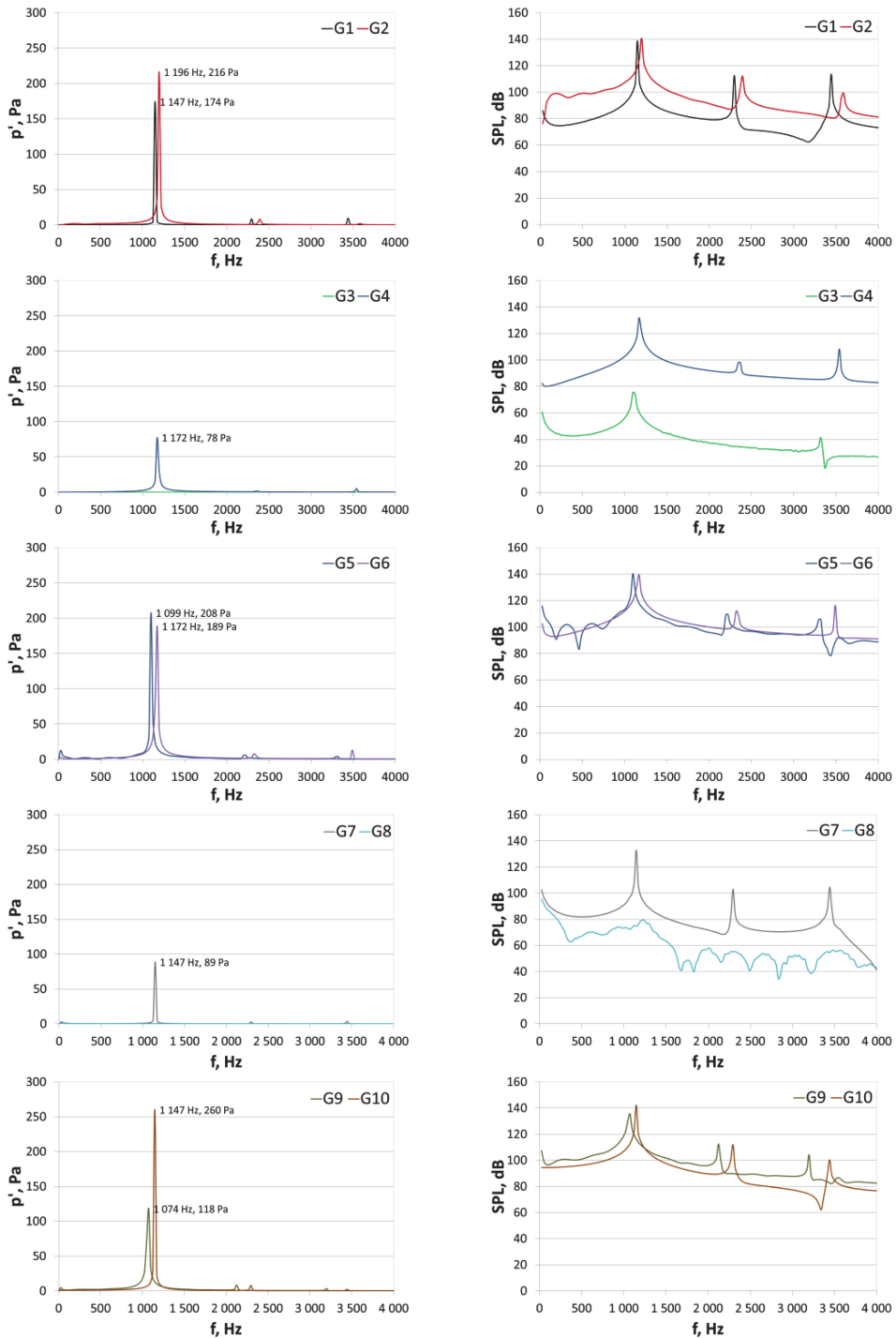
Fig. 5. Spectral analysis of pressure fluctuations and changes in the sound pressure level
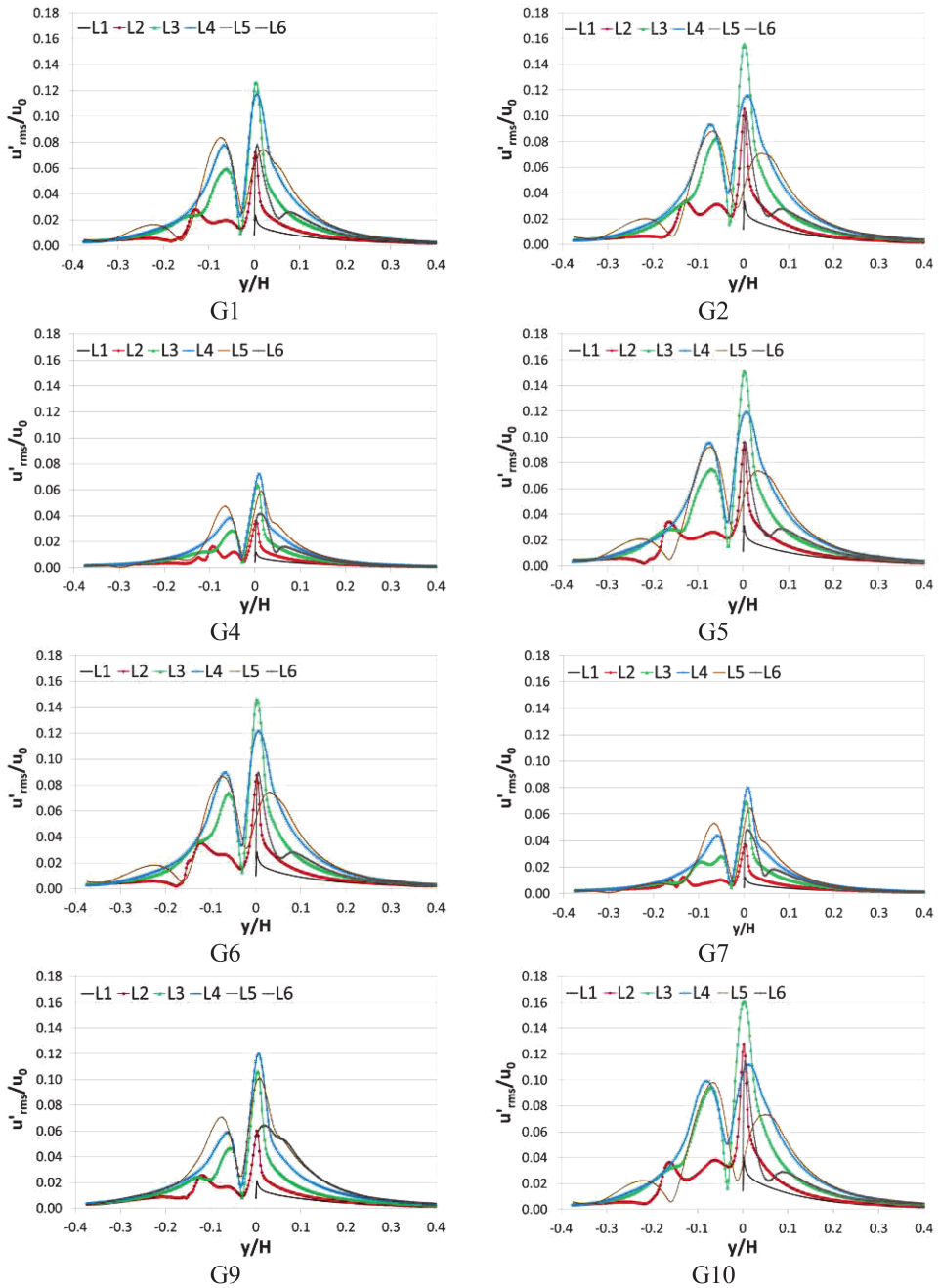
Fig. 6. RMS value of fluctuations in the horizontal component of velocity

of the considerable rise in the amplitude of acoustic oscillations, which is first and foremost related to the reduction in the cavity height and the increase in the vertical dimension of the cavity neck, geometrical configuration G10 was created. In it, both geometrical parameters are changed at the same time. In this case, the highest amplitude of acoustic oscillations was obtained of 260 Pa, which corresponds to 142 dB, at the frequency of 1147 Hz. This amplitude is by 86 Pa higher compared to initial configuration G1.

Fig. 6 presents the distribution of the normalized root-mean-square (RMS) value of fluctuations in the velocity horizontal component in the vortex path generated from the cavity leading edge onwards for six cross-sections L1–L6 shown in Fig. 2. Because no essential amplitude of acoustic oscillations was observed for configurations G3 and G8, the two cases are omitted in Fig. 6. For all the configurations under analysis, the position of the cross-sections is the same. Line L1 is in the point of the flow separation on the cavity leading edge, whereas line L6 is on the trailing edge. Configuration G9 is an exception. In it, line L6 is one cross-section upstream the trailing edge due to the bigger width of the cavity neck and the need to keep identical positions of the cross-sections in every case. Relative height y/H is defined in relation to the height of the main channel.

The history of the RMS values of velocity fluctuations indicates that the highest velocity fluctuation value for most of the cases under consideration is obtained within cross-sections L3 and L4, which are located in the middle part of the cavity neck width. For configuration G9, the area covers cross-sections L3–L5, which is related to the increase in the cavity neck width. For the final geometry (G10), the area of the maximum RMS values of velocity fluctuations is shifted towards the cavity leading edge and covers cross-sections L2 and L3. The maximum RMS value of velocity fluctuations for configuration G10 was obtained in cross-section L3. It exceeds 0.16. The shape of the distribution of fluctuations is in every case characterized by the lack of symmetry relative to the line $y/H = 0$ in all the cross-sections. The fluctuation distribution asymmetry is the greatest within the cross-sections where the maximum values of velocity fluctuations were obtained.

Fig. 7 and Fig. 8 present the evolution in time of the vorticity for initial geometry G1 and final geometry G10, respectively. Only four instantaneous states of a single period of changes are presented. It can be seen that, for initial geometry G1, a vortex in the area of the cavity neck width is formed later compared to configuration G10. For this reason, in the case of configuration G10 the vortex is fully formed before it hits the cavity trailing edge and gets split on it. It should also be noted that the circulation area for configuration G1 does not include the bottom part of the cavity chamber and reaches only 2/3 of the cavity height. In configurations where the cavity depth is reduced, such as G10 for example, the cavity walls in the cavity bottom area are washed by a portion of air flowing downwards, and the circulation itself is more intense. A stronger flow of vortices then occurs from the bottom corner of the lid. An increase in the cavity neck height enables formation of two
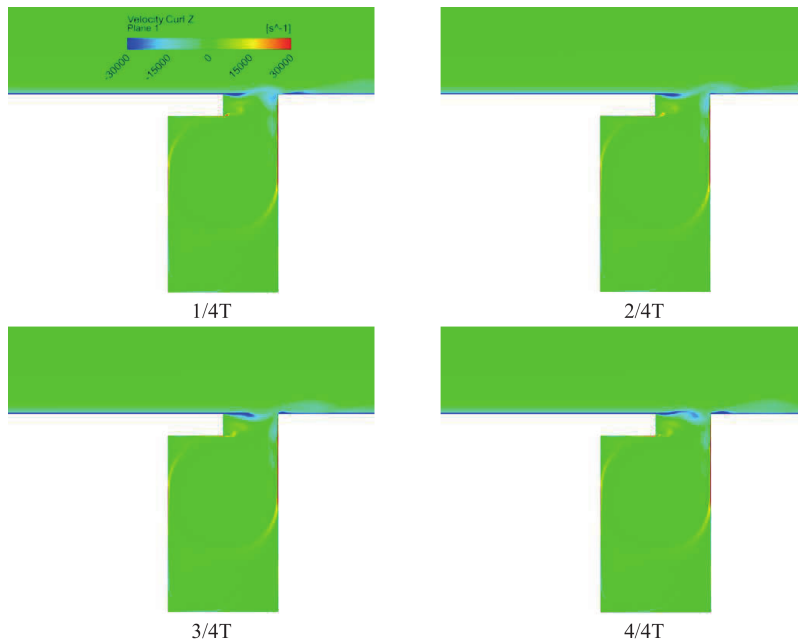
Fig. 7. Instantaneous distribution of the vorticity field for the initial geometry (G1)
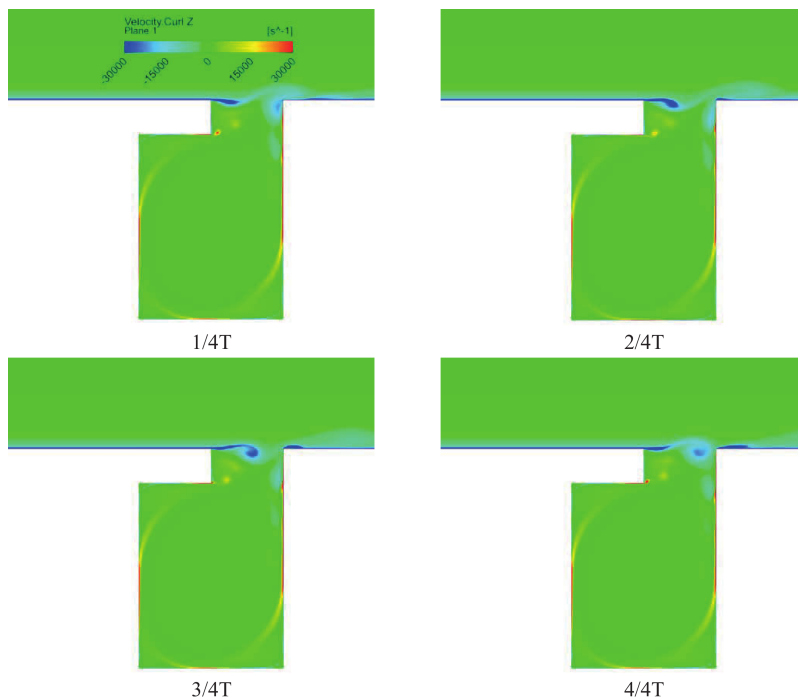

Fig. 8. Instantaneous distribution of the vorticity for the final modified geometry (G10)

vortices moving from the bottom of the cavity neck towards the main vortex path. This involves a rise in the velocity fluctuation values in the entire region of the cavity neck width.

Fig. 9 presents overpressure pulsations in the cavity area that accompany the flow of vortices in the cavity neck region for configuration G10. It can be seen that fast changes in pressure occur simultaneously in the entire volume of the cavity.
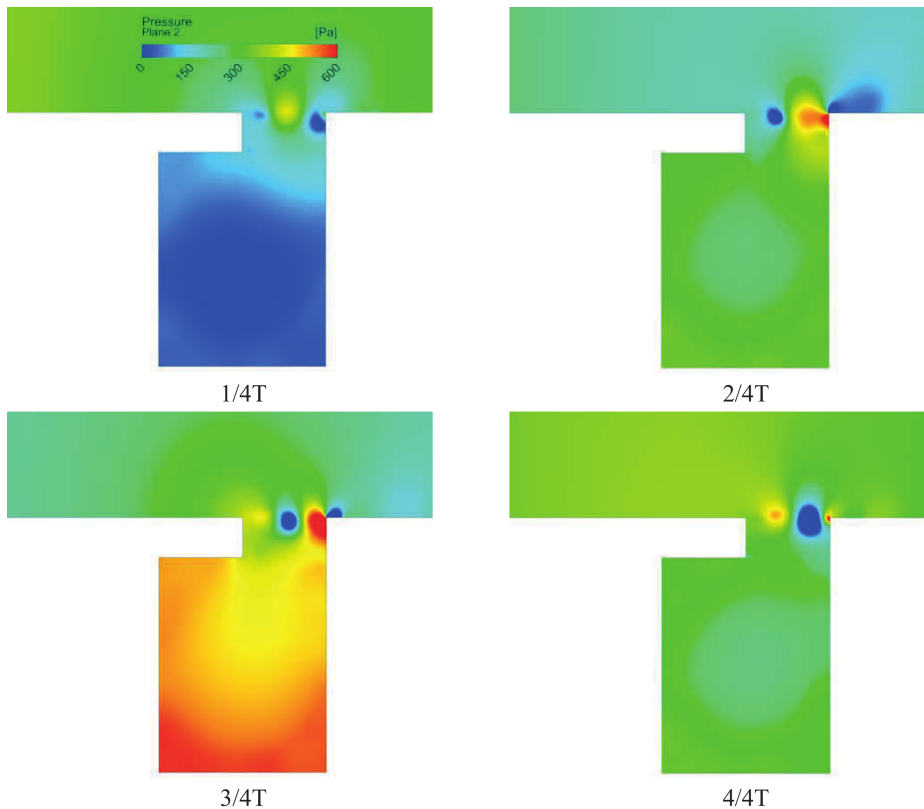
Fig. 9. Instantaneous distribution of overpressure for the modified geometry (G10)

High parameters of velocity fluctuations in the cavity neck region combined with a more intense circulation in the entire area of the cavity, as well as high pulsations in pressure, may contribute to a substantial improvement in the heat transfer conditions. For this reason, configuration G10 was selected for a further extended analysis aiming at defining the relation between the generated acoustic wave parameters and the heat transfer process taking place in the cavity region.

The flow boundary conditions in the extended analysis are the same as those assumed previously (cf. Table 1). The essential difference is that the Dirichlet boundary condition in the form of a constant temperature of 120°C (cf. Fig. 2) is assumed on the cavity walls.

The heat transfer efficiency in the cavity area was assessed using the heat transfer coefficient (HTC) defined as follows:

$$\text{HTC} = \frac{q}{T_{tot} - T_{\text{wall}}}, \qquad (8)$$

where: T_{wall} is the wall surface temperature. T_{tot} is total temperature of air at the inlet to the channel and is equal to 289.4 K.

The value of HTC at a given point of the cavity wall was determined as the arithmetic average calculated from the last 50 periods of parameter pulsations inside the acoustic generator.

Fig. 10 presents the distribution of the time-averaged temperature field for the initial configuration G1 and the final configuration G10. It can be seen that two stationary vortices rotating in opposite directions are formed inside the cavity for configuration G1. One covers the cavity top part, whereas the other, which is smaller, is located in the left-hand bottom part. In the case of configuration G10, there is one big vortex washing the cavity bottom wall and reducing the air temperature in this region substantially. In order to make a quantitative comparison of the heat transfer conditions, distributions of the heat transfer coefficient (HTC) defined according to (8) are presented.
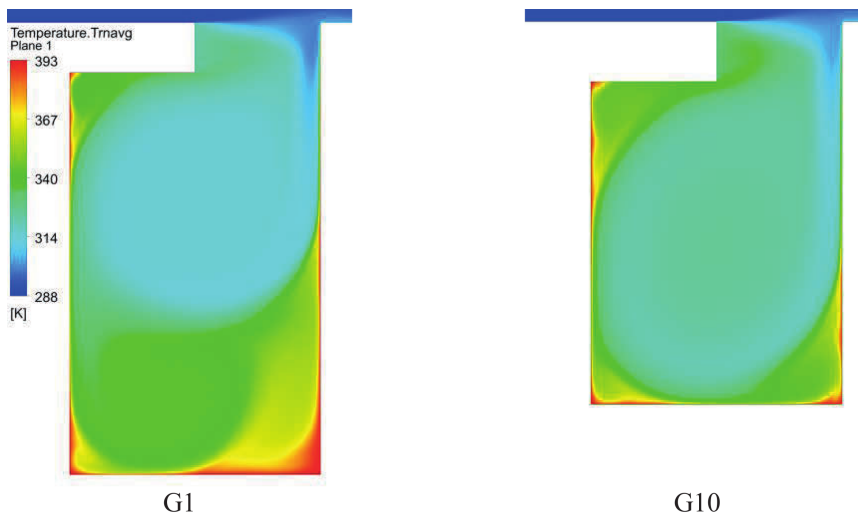

G1   G10

Fig. 10. Distribution of the time-averaged temperature field for initial and final configuration G1 and G10, respectively

Fig. 11 and Fig. 12 show the distribution of the HTC values for individual walls of the cavity for the initial configuration (G1) and the final configuration (G10), respectively. An additional comparison is also made between the HTC values obtained from the transient and the steady simulation. The obtained re-
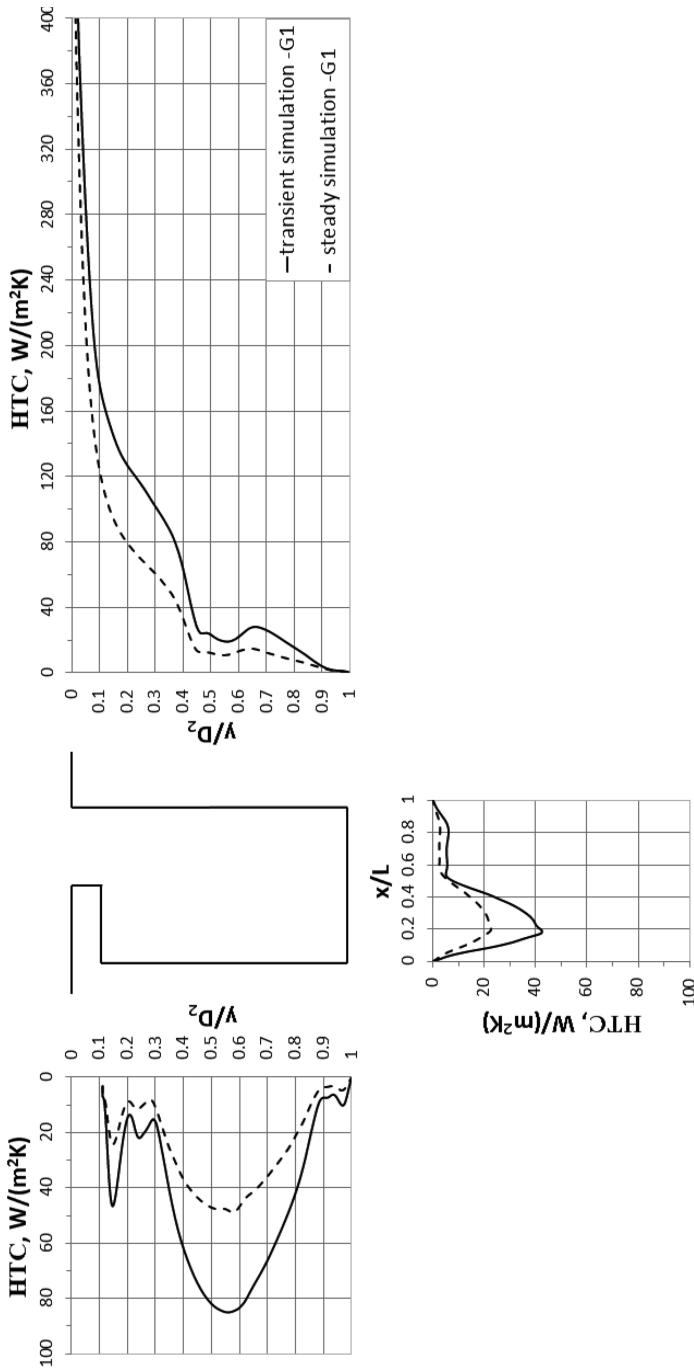
Fig. 11. Distribution of the HTC values for the cavity individual walls – configuration G1
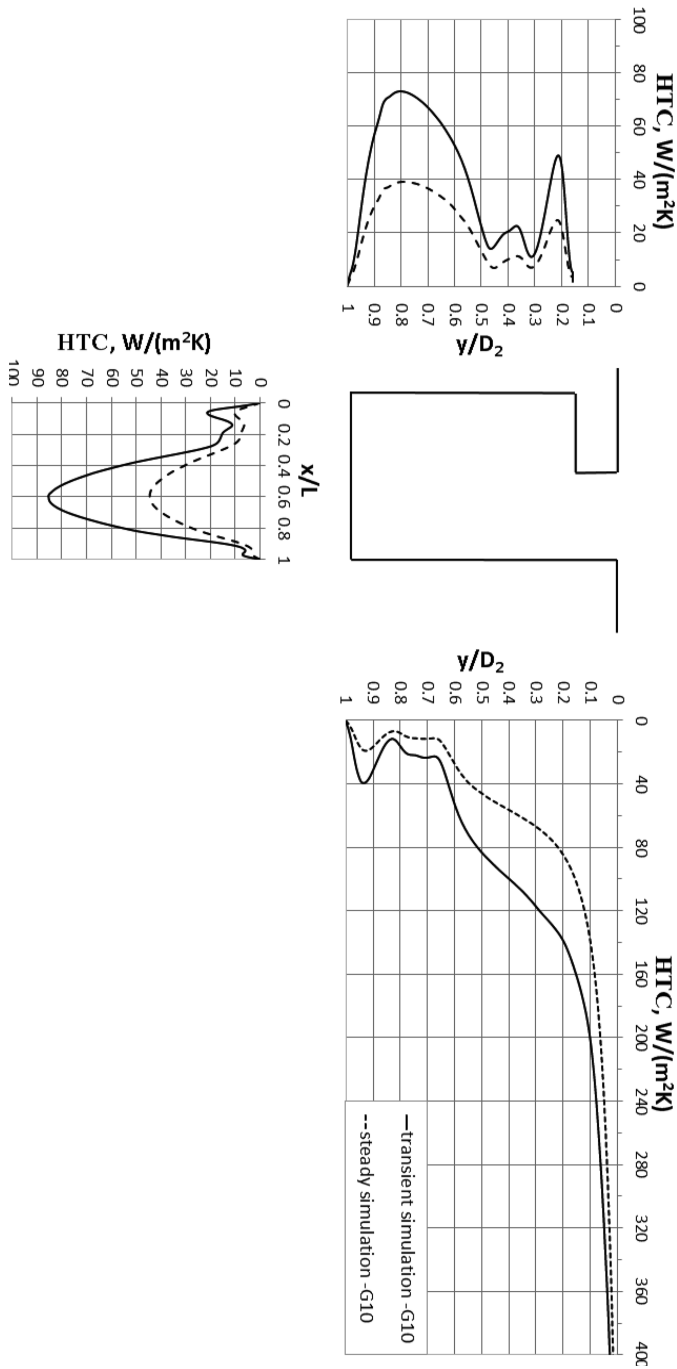
Fig. 12. Distribution of the HTC values for the cavity individual walls – configuration G10

sults differ from each other considerably, which may prove a significant impact of non-stationary effects on the heat transfer conditions. The highest value of the heat transfer coefficient was obtained for the right wall of the cavity. Intense cooling, especially of the wall upper part, occurs in this place, and the heat transfer coefficient reaches a value exceeding 500 W/(m^{2}K). The curves illustrating the HTC values for the two configurations under consideration have a very similar shape. Slight differences can be noticed in the cavity corner area. For configuration G10, a rise occurs in this place in the HTC value, reaching the level of 40 W/(m^{2}K). This is due to the formation of a small vortex within the cavity right corner. Considering the cavity left wall, it can be noticed that the obtained maximum HTC value is a little smaller for configuration G10 compared to configuration G1 (73 W/(m^{2}K) and 85 W/(m^{2}K), respectively). For configuration G10, the HTC value rises faster as the distance from the cavity bottom left-hand corner increases.

Compared to the initial configuration (G1), the highest increase in the HTC value was obtained for the cavity bottom wall. For configuration G1 the HTC maximum value was 42 W/(m^{2}K), whereas for configuration G10 it reached as high as 85 W/(m^{2}K).

Fig. 13 presents the area-averaged values of the heat transfer coefficient distribution presented in Fig. 11 and Fig. 12 and calculated for the cavity right, bottom and left wall (RW, BW and LW, respectively). The HTC average value for the cavity bottom wall in configuration G10 is 2.7 times higher compared to configuration G1. The HTC average value for the cavity right wall for configuration G10 is by 25% higher compared to configuration G1. A slight drop in the HTC average value by about 10% was obtained only for the left wall of the cavity.
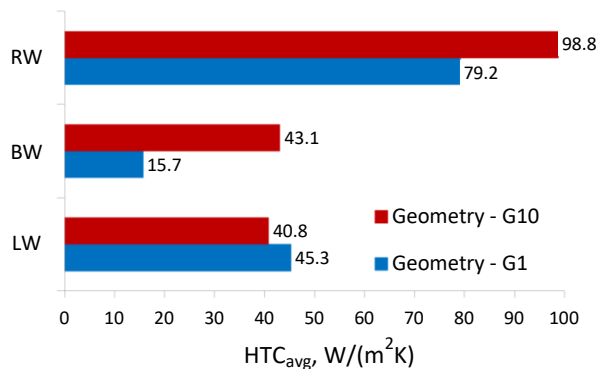

Fig. 13. HTC average value for individual walls of the cavity

The presented results indicate that appropriate selection of the acoustic generator geometrical parameters can produce a considerable improvement in the heat transfer conditions in the cavity area.

5. Summary and conclusions

The studies presented within this paper have a fundamental character. They are focused on quantitative analysis of heat exchange process under the influence of unsteady phenomena.

Numerical analysis of different geometrical configurations of the acoustic generator is made. Based on the results, a geometry is proposed that makes it possible to achieve the highest pulsations in pressure in the cavity area. The configuration was obtained by reducing the cavity depth and increasing the cavity neck height at the same time. The effect of this solution is that a more intense vortex is created inside the cavity compared to the initial configuration.

The results of the calculations of the heat transfer conditions performed for the modified geometry of the acoustic generator demonstrate a considerable rise in the heat transfer coefficient value compared to the initial configuration. The highest increase in the HTC average value was obtained for the cavity bottom wall. The values totalled 15.7 W/(m^{2}K) and 43.1 W/(m^{2}K) for the initial and the modified geometry, respectively. For the cavity right wall, the respective HTC values were 79.2 W/(m^{2}K) and 98.8 W/(m^{2}K). A slight drop of 4.5 (W/m^{2}K) was obtained only for the cavity left wall.

The performed analyses indicate that the search for the optimal shape of the cavity to achieve a further improvement in the heat transfer conditions is fully justified. Such geometrical features as the rounding of the cavity corners, for example, may substantially improve the heat transfer coefficient value in stagnation regions.

The results of the works presented herein point to the potential of making use of the non-stationary effects related to the process of the acoustic wave generation to improve the heat transfer conditions. In order to achieve such an improvement, the acoustic generator geometry has to be adjusted to the flow conditions in the main channel. Further research will focus on validation of the numerical analysis results and miniaturization of the presented solution.

Acknowledgements

References

[1] E.Y. Choi, Y.D. Choi, W.S. Lee, J.T. Chung, and J.S. Kwak. Heat transfer augmentation using a rib-dimple compound cooling technique. *Applied Thermal Engineering*, 51(1–2):435–441, 2013. doi: 10.1016/j.applthermaleng.2012.09.041.

[2] Z. Shen, Y. Xie, and D. Zhang. Experimental and numerical study on heat transfer in trailing edge cooling passages with dimples/protrusions under the effect of side wall slot ejection. *International Journal of heat and Mass Transfer*, 92:1218–1235, 2016. doi: 10.1016/j.ijheatmasstransfer.2015.09.042.

[3] Y. Rao, B. Li, and Y. Feng. Heat transfer of turbulent flow over surfaces with spherical dimples and teardrop dimples. *Experimental Thermal and Fluid Science*, 61:201–209, 2015. doi: 10.1016/j.expthermflusci.2014.10.030.

[4] C. Wang, L. Wang, and B. Sunden. Heat transfer and pressure drop in a smooth and ribbed turn region of a two-pass channel. *Applied Thermal Engineering*, 85:225–233, 2015. doi: 10.1016/j.applthermaleng.2015.03.079.

[5] J. Zhou, Y. Wang, G. Middelberg, and H. Herwig. Unsteady jet impingement: Heat transfer on smooth and non-smooth surfaces. *International Communications in Heat and Mass Transfer*, 36(2):103–110, 2009. doi: 10.1016/j.icheatmasstransfer.2008.10.020.

[6] G. Middelberg and H. Herwig. *Heat transfer under unsteadily impinging jets: a systematic investigation.* In *Proc. 13th International Heat Transfer Conference*, Sydney, Australia, 2006.

[7] S. Göppert, T. Gürtler, H. Mocikat, and H. Herwig. Heat transfer under a precessing jet: effects of unsteady jet impingement. *International Journal of Heat and Mass Transfer*, 47(12–13):2795–2806, 2004. doi: 10.1016/j.ijheatmasstransfer.2003.11.026.

[8] L. Larcheveque, P. Comte, and P. Sagaut. Large-eddy simulation of flows past cavities. *AFM research group seminar*, Southampton, February 25, 2004.

[9] L. Larcheveque, P. Sagaut, I. Mary, and O. Labbe. Large-eddy simulation of a compressible flow past a deep cavity. *Physics of Fluids*, 15(1):193–210, 2002. doi: 10.1063/1.1522379.

[10] S. Rulik, W. Wróblewski, G. Nowak, and J. Szwedowicz. Heat transfer intensification using acoustic waves in a cavity. *Energy*, 87:21–30, 2015. doi: 10.1016/j.energy.2015.04.088.

[11] S. Rulik and W. Wróblewski. A numerical study of the heat transfer intensification using high amplitude acoustic waves. (in print).

[12] W. Wróblewski and K. Bochon. Conjugate heat transfer analysis of the tip seal in the counter rotating low pressure turbine. *Archives of Mechanics*, 67(3):253–270, 2015.

[13] D. Spura, J. Lueckert, S. Schoene, and U. Gampe. Concept development for the experimental investigation of forced convection heat transfer in circumferential cavities with variable geometry. *International Journal of Thermal Sciences*, 96:277–289, 2015. doi: 10.1016/j.ijthermalsci.2014.08.018.

[14] E.J. Rossiter. Wind tunnel experiments on the flow over rectangular cavities at subsonic and transonic speeds. Royal Aircraft Establishment, RAE Farnborough, Technical Report No. 64037, 1964.

[15] Ö.H. Ünalmis, N.T. Clemens, and D.S. Dolling. Cavity oscillation mechanisms in high-speed flows. *AIAA Journal*, 42(10):2035–2041, 2004. doi: 10.2514/1.1000.

[16] A.T. de Jong and H. Bijl. Investigation of higher spanwise Helmholtz resonance modes in slender covered cavities. *The Journal of the Acoustical Society of America*, 128(4):1668–1678, 2010. doi: 10.1121/1.3473698.

[17] F.R. Menter. Zonal two-equation $k - \omega$ turbulence model for aerodynamic flows. AIAA Paper 93-2906, 1993.

[18] F.R. Menter. Two-equation eddy-viscosity turbulence models for engineering applications. *AIAA-Journal*, 32(8):1598–1605, 1994. doi: 10.2514/3.12149.

[19] S. Dykas, W. Wróblewski, S. Rulik, and T. Chmielniak. Numerical modeling of the acoustic waves propagation *Archives of Acoustics*, 35(1):35–48, 2010.

[20] B. Henderson. Automobile noise involving feedback-sound generation by low speed cavity flows. *Third Computational Aeroacoustics (CAA) Workshop on Benchmark Problems*. NASA/CP-2000-209790, 95–100, 2000.

[21] *Third Computational Aeroacoustics (CAA) Workshop on Benchmark Problems*, NASA/CP–2000-209790.

[22] *Fourth Computational Aeroacoustics (CAA) Workshop on Benchmark Problems*, NASA/CP–2004-212954.